DESIGN AND ASSEMBLY OF AN ULTRASONIC FATIGUE TESTING MACHINE

M. Freitas, L. Reis, V. Anes, D. Montalvão, A. M. Ribeiro and M. Fonte

ICEMS & Dept. of Mechanical Engineering, Instituto Superior Técnico
Av. Rovisco Pais, 1049-001 Lisboa, Portugal.
E-mail: mfreitas@dem.ist.utl.pt; luis.g.reis@ist.utl.pt

RESUMEN

El periodo de vida de estructuras sometidas a cargas cíclicas esta basado en las curvas S_N, que establecen un tiempo de vida infinito cuando el esfuerzo aplicado es menor que la resistencia limite. Estudios demuestran que el colapso debido a fatiga es alcanzado después de 10e7 ciclos, indicando que no hay resistencia límite de fatiga. Sin embargo, la obtención de estas cargas límite a través de máquinas servo hidráulicas requiere mucho tiempo. De esta manera, las maquinas ultrasónicas para predecir fatiga están diseñadas para conducir ensayos en un periodo de tiempo mucho menor. El presente trabajo describe el diseño y montaje de un dispositivo para ensayos ultrasónicos de fatiga a 20kHz.

ABSTRACT

The lifetime approach in fatigue design based on S_N curves establish an infinite life when the cyclic stress applied is below than the endurance limit. Results in this field revealed fatigue failures beyond 10e7 cycles, indicating that there´s no endurance fatigue limit, however obtaining this data with servo-hydraulic testing machine can be very time-consuming and expensive. Ultrasonic fatigue testing machines are a new generation of devices designed to perform VHCF tests in a very short time. This paper describes the design and assembly of an ultrasonic fatigue testing device working at 20 kHz.

KEYWORDS: Giga cycle fatigue; Ultrasonic fatigue; Experimental tests; VHCF.

1. INTRODUCTION

In mechanical design the S_N diagrams are used to dimension metallic components in order to resist a given number of load cycles. The data used to create these diagrams is acquired in the laboratory by performing cyclic tests until the rupture. The classic fatigue test equipment has some operational restrictions due to the technology used in the design of those machines. These limitations were observed until 1980s, and are mainly based on the time spend in the cyclic tests. Due to this issue the number of testing cycles was generally limited to 10e6 to 10e71, reaching a stress limit. The limit was named “endurance limit” which is a horizontal line defined beyond 10e6 cycles in the S_N diagram. This limit led to infinite fatigue lives if the cyclic loading is under that limit [1, 2]. This was well accepted until the 1970s. However, the emergence of new productive technologies and materials increase the required fatigue life range being necessary fatigue data beyond the specific cycles to design mechanical components. Nevertheless, it was observed fatigue failures beyond 10e6 cycles, which led to conclude the necessity to improve the S_N diagrams and eliminate the endurance limit [3, 4]. Nowadays, the conventional fatigue testing machines are hydraulic or electric with maximum working frequency at 100 Hz, which means four testing months to reach 10e9 cycles being unaffordable this testing regime.

The improvements in the piezoelectric actuators and signal generators lead to the creation of the new generation of testing machines called ultrasonic fatigue test machines working at 20 kHz, reaching 10e9 cycles in fourteen hours [5]. The ultrasonic testing was applied for the first time by Hopkinson at very beginning of the last century, until 1911 the highest testing frequency reached was 33 Hz. The fatigue test mechanisms were completely mechanical at that time. After that Hopkinson designed an electromagnetic system using the resonance principles reaching the highest frequency of 116 Hz. Fourteen years lather Jenkin test a wide number of materials at the frequency of 2.5 kHz using ultrasonic techniques. In the 1930s Jenkin and Lehmann improved the pneumatic testing machine reaching 10 kHz as testing frequency. Twenty years after that, in 1950, a benchmarked was reached. Manson created the first piezoelectric testing machine and developed important ultrasonic fatigue testing techniques. He used a piezoelectric transducer commanded by an electrical voltage signal with a 20 kHz frequency and was capable of inducing fatigue fracture at the ultrasonic regime [6].

New proposals for ultrasonic testing machines appeared in the last decades with higher frequencies reaching 199 kHz in the year of 1965 by Kikukawa. The increasing of

frequency has some issues with difficult handling, for instance, the frequency increase lead to a decrease of the geometrical dimensions and a higher rate in the heat generation [7, 8]. Therefore, the design of Manson´s 20 kHz machine still is the basis of the actual research in the ultrasonic testing machines. The idea of using the ultrasonic technology in the determination of S_N curves initiate in 1959 with Neppiras and still present nowadays. This approach leads to a new research field with the purpose to measuring the fatigue life under a very high number of cycles.

Despite having deep investigations around the VHCF only few research teams are working in the design and assembly of this kind of testing machines. The technical information about these methodologies and mechanisms are still restricted. Therefore, the objective of design and assembly an ultrasonic machine with 20 kHz as working frequency, was established and successfully achieved. There are three main systems in the setup implemented; the resonant system, the data acquisition and the temperature control. The resonant system is composed by one piezoelectric actuator, a signal generator, one booster, a horn and a specimen test. The actuator is a device which transforms the electrical signal into mechanical vibration. The actuator is commanded by a signal generator who converts 50 Hz voltage into an electric sinusoidal signal with the system resonance frequency.

The booster and horn amplify the vibration coming from the transducer in order to obtain the required stress amplitude in the middle section of the specimen. The specimen test is a kind of horn with the particularity to be symmetric relatively to the middle of longitudinal dimension, unlike other elements this resonant element is disposable and is used only once. The horn and specimen´s test were designed and machined in the workshop. The design was developed with finite element routine procedures, having as output the geometry of the resonant element with 20 kHz as resonant frequency at longitudinal mode of vibration. Due to the variance in the material's properties, the design strategy provided locations in the element geometry to make adjustments in order to achieve the desired resonant frequency. The other resonant components were purchased in the market and adapted to the machine.

The piezoelectric actuator, booster and signal generator used were acquired from Branson. One control box was created to adapt the signal generator and permit the connection to the PC where the control of the fatigue machine is carried out. The data acquisition system is composed by one laser and one DAQ with 400 kS/s as sample rate. The cooling system is composed by one pyrometer and one vortex, which are controlled by one labVIEW routine.

2. DESIGN & ASSEMBLY

2.1 Acoustical Design

The ultrasonic energy must be transmitted between resonant elements in an efficient way. This efficiency can be achieved due to the amplification granted by specific geometric properties of the elements at the longitudinal mode. That amplification lays down in one transmission line along the elements, starting in the actuator and ending at the specimen bottom. Along this line is provided a change in the amplitude of vibration, which means different levels of axial tension along all elements [9]. In Figure 1 is represented the booster, horn and specimen with the typical evolution of displacement and stress along the amplification line.

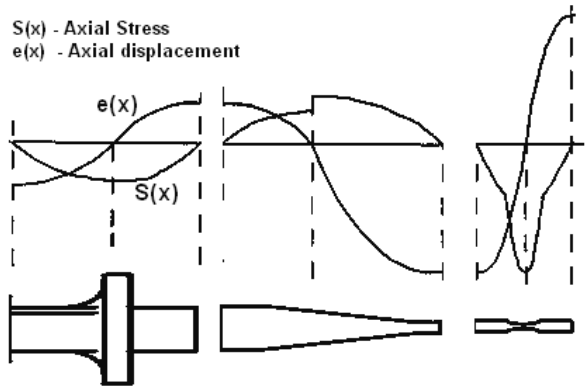

Figure 1. Amplification line along the elements.

The design of ultrasonic elements has two major categories; slender and wide area elements. The difference between them is the Poisson effect. In the slender elements, this effect may be neglected, but in wide area elements this effect must be considered, for instance in the design of a specimen test the Poisson effect can be neglected, but not with some horns.

Therefore, neglecting the Poisson´s effect leads to consider the acoustical waves propagating along the axial axis of the element in a flat form. Thus, the displacement along the axis perpendicular to the axial axis can be neglected. This assumption leads to another consideration; the ultrasonic energy is distributed uniformly along each cross sectional area only changing with the axial distance to the source.

Meanwhile, slender elements are desirable in ultrasonic fatigue testing, to prevent radiation normal to the surface which means a reduction of the effectiveness of the horn and a loss of ultrasonic energy [9].

The flat waves can be assumed in one taper horn if the contour is sufficiently gradual, this issue determines the acoustical behaviour in the transmission line and determines the effectiveness of the element, because of that the stepped horn has a huge of ultrasonic loses.

Considering the geometry of the specimen test, at the variable section zone, different amplitudes of strain and stress will be achieved varying section to section. In the specimen throat, the axial section is the most reduced in

order to achieve the maximum axial stress. Some geometries can be determined with differential equations but are limited to specific contour, such as: exponential or hyperbolic. The tapered horn is the easiest solution to produce in the laboratory but the geometry is only achieved by numerical tools like FEM. The standard specimen test, Figure 2, has an exponential throat and two cylindrical zones which length is regularly named as resonance length. The specimen geometry can be achieved as follows:

2.2 Analytical Specimen Design

Under longitudinal resonance, the specimen behaviour must satisfy the differential equation 1, determined by the equilibrium of forces.

$$\frac{\partial^2 u(x,t)}{\partial x^2} + P(x)\frac{\partial u(x,t)}{\partial x} = \frac{1}{C^2}\frac{\partial^2 u(x,t)}{\partial t^2} \tag{1}$$

Considering the follow variable change, applied to equation 1.

$$u(x,t) = U(x)\sin(wt) \tag{2}$$

The amplitude of vibration U(x) at each point along the specimen can be easily obtained by:

$$U''(x) + P(x)U'(x) = -\frac{w^2}{C^2}U(x) \tag{3}$$

Considering the appropriated boundary conditions in the specimen, see Figure 2, the differential solution divided in two parts is achieved, see equations 4 and 5.

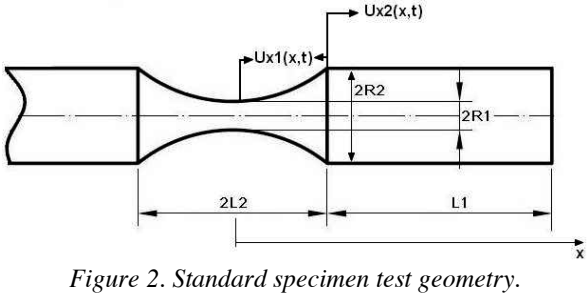

Figure 2. Standard specimen test geometry.

$$U_1(x) = \frac{C_1\exp(\beta x) + C_2\exp(-\beta x)}{\cosh(\alpha x)}, x < L_2 \tag{4}$$

$$U_2(x) = C_3\cos(kx) + C_4\sin(kx), L_2 < x \le L \tag{5}$$

The constants C1, C2, C3 and C4 are determined with the resonant boundary conditions. Equations 6 and 7 represent the displacement behaviour at longitudinal mode.

$$u_1(x,t) = \frac{A_0\cos(kL_1)\cosh(\alpha L_2)}{\sinh(\beta L_2)}\frac{\sinh(\beta x)}{\cosh(\alpha x)}\sin(wt), x < L_2 \tag{6}$$

$$u_2(x,t) = A_0\cos(k(L-x))\sin(wt), L_2 < x \le L \tag{7}$$

These two solutions represent the longitudinal resonance regime of the specimen in two different regions. In the interface between these regions the displacement must be the same.

$$u_1(x = L_2, t) = u_2(x = L_2, t) \tag{8}$$

Therefore selecting a value for the hyperbolic length, L2, the expression for the cylindrical length is achieved. It is reached easily the characteristic dimension of the specimen test with the equations 9 to 13.

$$L_1 = \frac{1}{k}arctg\left[\frac{\beta\coth(\beta L_2) - \alpha\tanh(\alpha L_2)}{k}\right] \tag{9}$$

$$\alpha = \frac{1}{L2}\arccos h\left(\frac{R_2}{R_1}\right) \tag{10}$$

$$k = \sqrt{\frac{w^2}{C^2}} \tag{11}$$

$$\beta = \sqrt{\alpha^2 - k^2} \tag{12}$$

$$C = \sqrt{\frac{E_d}{\rho}} \tag{13}$$

Were ***w*** is the resonance frequency in rad/s. In Figure 3 is represented the one specimen test dimensions made with 42CrMo4.

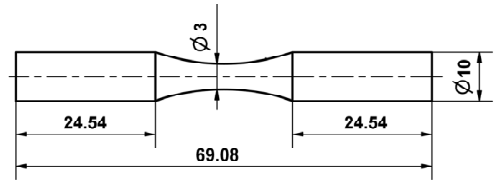

Figure 3. Standard specimen test geometry and dimensions.

The horn geometry is determined using the same approach used in the specimen test; the contour is defined with the ratio P(x) defined in equation 3. In equation 14 the length of exponential horn can be determined in function of the sectional areas at extremities, S1 and S2,

$$L_n = \frac{C}{2f_n}\sqrt{1 + tag\left(\frac{1}{2\pi}Ln\left(\frac{S_2}{S_1}\right)\right)^2}; S_2 < S_1 \tag{14}$$

2.3 3D FEM Modelling

The natural frequencies, mode shapes and the location of the nodal plane of the resonant elements were determined with a modal analysis computed in Ansys.
The FEM element used was the solid186, with the mechanical properties of 42CrMo4 steel. The mesh was implemented considering the smart mesh tool with level 5. The geometry was parameterized with tuning features

in some variables, allowing reaching the frequency and mode desirable by changing their values. The desired mode is identified by visual inspection. The natural frequency was computed using the block Lanczo's method. After the geometric design, the system assembly was computed with input simulation. The interface between elements was considered and adopted specific boundary conditions for each element [10, 11]. The system input was applied in the free extremity of the booster. This input considers the force applied with the resonant frequency of the system. The system was fixed in the middle of the booster were the nodal plan is well identified, and displacement is near zero.

2.4 Horn Design

Three types of contour were considered for the horn design geometry; it were considered the tapered, exponential and hyperbolic shape. Two cases were also considered, horns with and without cylindrical ends. In these six cases, the resonant geometries at 20 kHz were determined. In Figures 4, 5 and 6 are presented the geometric dimensions for the three cases with cylindrical ends.

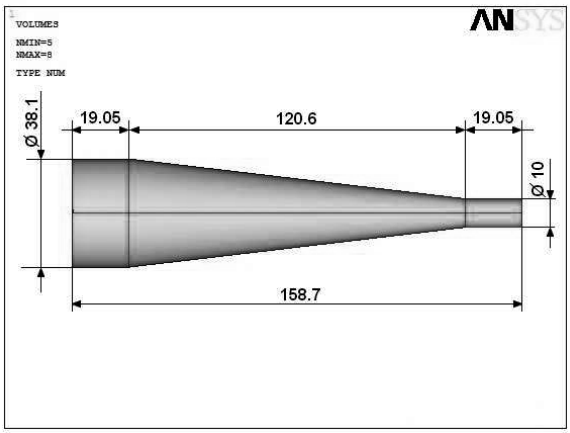

Figure 4. Tapered horn at 20 kHz

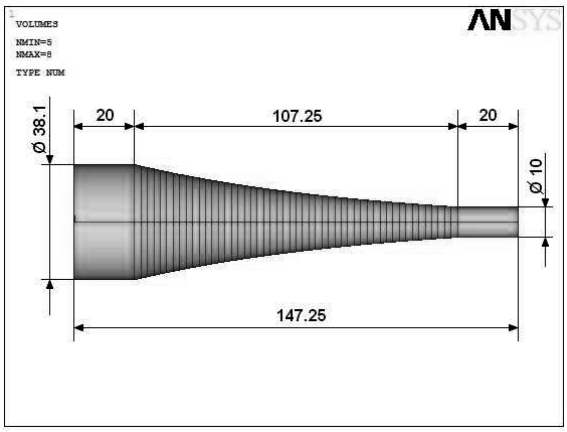

Figure 5. Exponential horn at 20 kHz.

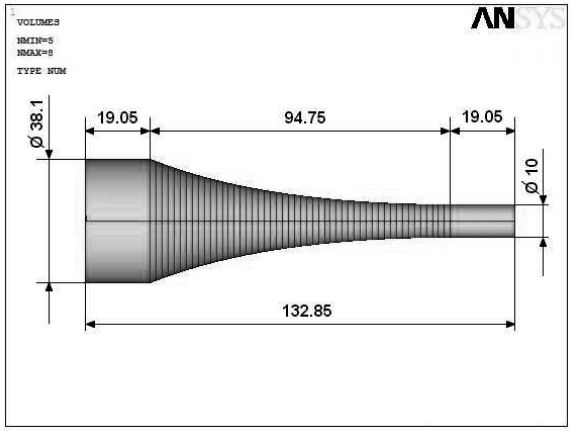

Figure 6. Hyperbolic horn at 20 kHz.

Modes with frequencies near the working frequency were computed, inspected and analysed for the six cases considered. Table 1 and Table 2 present the results achieved for each case.

Table 1. Frequency and modes around the working frequency 20 kHz; cases without cylindrical ends.

Shape	Length [mm]	Bending [Hz]	Working Axial [Hz]	Torque [Hz]
Tapered	148.26	19857	20000	21060
Exponential	140.46	19231	20000	20069
Hyperbolic	131.36	19237	20000	21004

Table 2. Frequency and modes around the working frequency 20kHz; cases with cylindrical ends.

Shape with	Length [mm]	Bending [Hz]	Working Axial [Hz]	Torque [Hz]
Tapered	158.7	22630	20000	19265
Exponential	147.25	22623	20000	19790
Hyperbolic	132.85	19407	20000	20716

The connectivity and the effect of material properties on the resonance frequency were analysed with an Ansys parameterization. The variables used “a” and “c” represent the cylindrical length and screw length, respectively. The connectivity between elements is implemented by a screwed joint; this solution has proven to be the best solution in terms of connectivity. In Figure 7 is represented the variable's location in the tapered horn. The effect of variation of the young modulus in the resonant layout was also considered. In Table 3 is presented the results from this analysis.

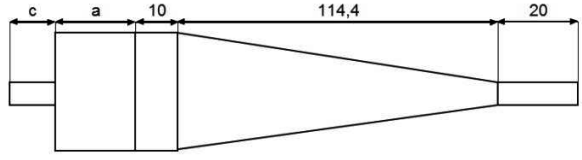

Figure 7. Tapered horn at 20 kHz with screw.

Table 3. Resonant frequency variation with Young modulus variation and geometric variables.

	Screw Length	**E 211 [GPa]**	**E 200 [GPa]**	
a [mm]	c [mm]	F [Hz]	F [Hz]	L Total [mm]
25	0	19400	18888	169,43
20	10	19687	19167	174,43
20	0	19781	19258	164,43
15	15	20051	19522	174,43
15	10	20102	19571	169,43
15	0	20213	19680	159,43
13	17	20198	19664	174,43
13	0	20388	19849	157,43
13	15		19685	172,43
10	10		19998	164,43
5	10		20460	159,43
5	20		20319	169,43

The selected geometrical shape for the horn and applied to the system is presented in Figure 8, the dimensions are in mm. The horn design has considered adjustments in the length to tune the frequency, in Figure 8 is represented the location and the variation behaviour of the variable adjust. The displacement amplification achieved is 3.

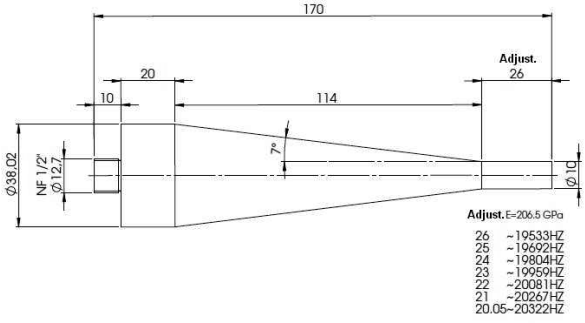

Figure 8. Tapered horn designed with adjustment (mm).

2.5 Specimen Design

The main objective concerning the specimen design, besides having the resonance frequency of the system, was creating a simple geometry to fabricate at the laboratory. The hyperbolic or exponential throats have a contour difficult to make with a conventional lathe, thus due to the number of specimen test required this solution is more adequate. With this geometry the tuning is made at the bottom of the specimen.

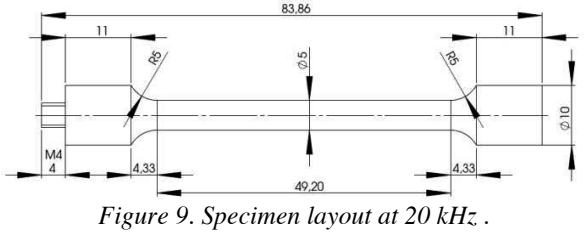

Figure 9. Specimen layout at 20 kHz .

The system was computed in an Ansys routine. The system input was applied to the booster with sinusoidal frequency at resonance value. At the specimen throat, the stress achieved was 480 MPa, see Figure 10, for 2.65 MPa at the interface between the actuator and the booster.

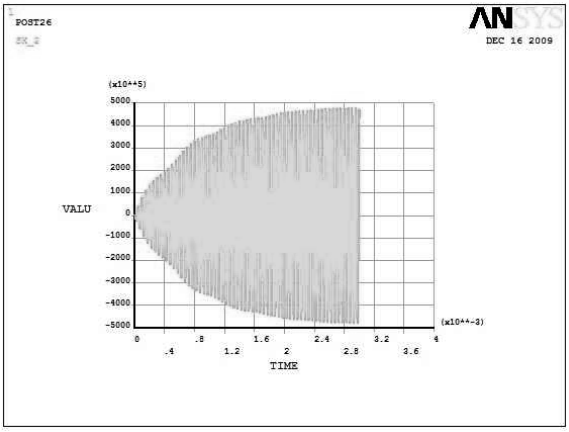

Figure 10. Axial stress evolution at the specimen throat.

3. RESULTS & DISCUSSION

3.1 Results

In Figure 11 is presented the resonant system designed and assembled. The elements; actuator, booster, horn and specimen test were linked together with a screwed connection with appropriated torque to avoid the premature degradation of the connections.

Figure 11. Resonant fatigue test system.

In Figure 12, the frequency scan shows the resonance frequency of the entire system at 20 kHz.

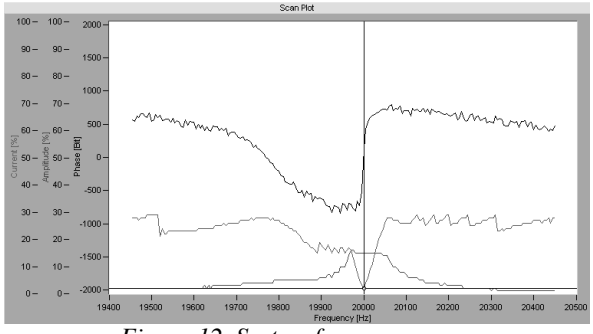

Figure 12. System frequency scan.

The resonance regime is identified when the actuator amplitude is maximum and the value for the electric current had the minimum value; at this stage, it occurs a phase change in the displacement behaviour. The displacement and the testing frequency at the specimen bottom were verified with the subsystem data acquisition. The amplification factor and the working frequency match with the numerical estimations. In Figure 13 is shown the layout of the lab VIEW programme; with this routine it is possible identify and control the working frequency, actuator amplitude, specimen amplitude and temperature monitoring.

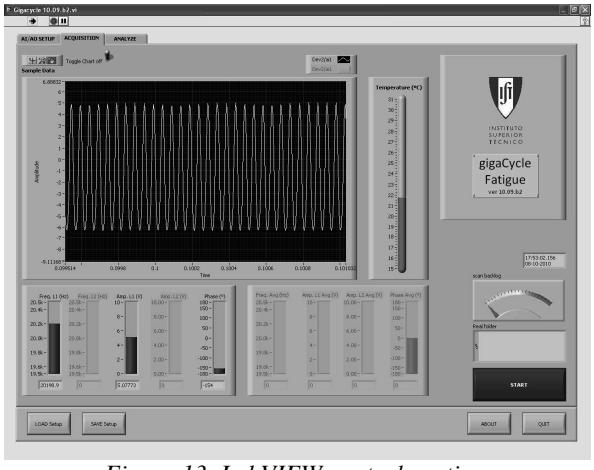

Figure 13. LabVIEW control routine.

3.2 Discussion

During the test process it is necessary to avoid the activation of the vibrating modes around the working mode due to issues related with security and with loading type. The modes of vibrations around the axial mode must have frequencies the farthest as possible from the resonant system frequency. From Table 1 the best solution in terms of safety and reliability is the hyperbolic case. Vibration's modes have in this case the values more distanced from the working frequency. However, the connectivity zone between the horn and the actuator has reduced fatigue strength in these cases. To increase the fatigue strength was considered two cylindrical body´s on extremities of the horn layout. These approach leads to increase the gap between resonance frequency´s from the different modes near the working mode, in this case the best solutions is the tapered horn, see Table 2. Due to this improvement and ease of machining this solution was selected. The Young modulus influence in the resonance frequency was presented in Table 3. For the same geometry reducing the Young modulus will reduce the resonance frequency. The screw presence in the tapered horn increases about 100 Hz in the frequency value, but doubling the screw length will increase 500 Hz. The length is not the only variable to determine the resonant frequency, for instance, in the Table 3, the first and the last case have the same length but the frequencies differ about 1400 Hz. Due to the uncertainties about the real Young modulus, machining, connections variables or material imperfections it is necessary to establish tuning points on the geometry. These adjustments must allow an increase or decrease on the resonant frequency.

4. CONCLUSION

The optimized geometries for the horn and specimen were defined and produced in the laboratory. The resonant system was assembled and was verified the resonant condition in the system. The material properties have a huge influence in the resonance frequency, as well as the geometry shape. The design of resonant elements must consider tuning points in the geometry layout.

ACKNOWLEDGEMENTS

The authors gratefully acknowledge financial support from FCT - Fundação para Ciência e Tecnologia (Portuguese Foundation for Science and Technology), through the project PTDC/EME-PME/69904/2006.

REFERENCES

[1] Zettl B, Mayer H, Ede C and Stanzl-Tschegg S 2006 Int. J. Fatigue 28 1583-9.
[2] Mughrabi H 2006 Int. J. Fatigue 28 1501-8.
[3] Bathias C, Drouillac L, le Franc¸ois P. How and why the fatigue S–N curve does not approach a horizontal asymptote. Int J Fatigue 2001; 23:143–51.
[4] Bathias C. There is no infinite fatigue life in metallic materials. Fatigue Eng Mater Struct 1999; 22:559–65.
[5] R. Frederick, "Ultrasonic Engineering," John Wiely & Sons, Inc., New York, 1965.
[6] Wang QY. Etude de la fatigue gigacyclique des alliages ferreux. Ph.D. thesis. Ecole Centrale de Paris, Me´canique et Mate´riaux, Laboratoire de la Me´canique de la Rupture du CNAM (Conservatoire Nationale des Arts et Me´tiers de Paris), 1998.
[7] Wang QY, Berard JY, Dubarre A, Baudry G, Rathery S, Bathias C. Gigacycle fatigue of ferrous alloys. Fatigue Fract Eng Mater Struct 1999; 22:667–72.
[8] Bathias C 1999 Fatigue Fract. Eng. Mater. Struct. 22 559-65
[9] W.P. Mason, Electromechanical Transducers and Wave Filters, D. Van Nostrand, New York, 1942.
[10] R. Krimholtz, D.A. Leedom, G.L. Mattaei, "New equivalent circuits for elementary piezoelectric transducer" Electron. Lett. 6 (1970) 398-399.
[11] Jian S. Wang and Dale F. Ostergaard, "A Finite Element-Electric Circuit Coupled Simulation Method for Piezoelectric Transducer" IEEE Ultrasonics Symposium, Proceedings, Volume 2.